F.F. Komarov, A.M. Mironov

Carbon Nanotubes: Present and Future

Institute of Applied Physics Problems,
Belarussian State University, 220064, 7 Kurchatov St., Minsk, Belarus,
e-mail: KomarovF@bsu.by

Current methods for synthesizing and studying carbon nanotubes are reviewed. The correlation between the structural features and electronic, electrical, chemical and mechanical characteristics of carbon nanotubes is discussed. Recently developed methods for growing uniform arrays of aligned nanotubes tailored for specific properties are discussed, which hold promise for the mass production and world-wide application of nanotube devices. Current and potential applications of nanotubes are discussed.

Keywords: carbon nanotubes, structure, characterization, application.

Content

I. Introduction

The discovery and synthesis of carbon nanotubes have stimulated intensive studies for their potential application because of the unique mechanical and electronic properties of this class of materials (Table 1). Now, it is known that carbon nanotubes have superior mechanical strength and low weight (tensile modules ~ 1 TPa) [1] as well as good heat conductance (heat conductivity of multi-wall carbon nanotube (MWCNTs) bundles ~ 2000 W/mK) [2]. They could be either metallic or semiconducting, depending on their helicity and diameter [3, 4]. Perhaps the most intriguing property of single-wall carbon nanotubes (SWCNTs) is the high room temperature mobility of semiconducting SWCNTs that is more than an order of magnitude larger than the mobility of crystalline Si [5, 6]. A large surface area is useful for the adsorption of hydrogen or other gases (H_2 can be stored on 98 wt / % pure SWCNTs up to 7÷10 wt % [7, 8]). The ability to emit cold electrons at relatively low voltages is due to high aspect ratio and nanometer size tips as well as high mechanical strength and chemical stability [9]. These unique structures reveals thermal stability at 1400ºC in a vacuum [10].

Therefore, carbon nanotubes have great potential for applications to field-emitters for flat-panel field-emission displays [11] and vacuum microelectronic devices such as microwave power amplifier tubes [12], field-effect nano-transistors (FETs), nano-schottky diodes, ion storage batteries and mechanical structures (composite materials) requiring low weight and high strength (Table 1).

II. Structural properties of CNTs

It is the chemical genius of carbon that it can bond in different ways to create structures with entirely different properties. Graphite and diamond, the two bulk solid phases of pure carbon, bear testimony of this. The mystery lies in the different hybridization that carbon atoms can assume. The four valence electrons in carbon, when shared equally (sp^3 hybridization), create isotropically strong diamond. But when only three electrons are shared covalently between neighbors in a plane and the fourth is allowed to be delocalized among all atoms, the resulting material is graphite. The latter (sp^2) type of bonding builds a layered structure with strong in-plane bounds and weak out-of-plane bonding of

Table 1

Physical properties of CNTs and device structures

Type of CNTS	Property	Quantity	References
SWCNT	density	~0.6 g/cm^3	[14]
MWCNT	density	~1–2 g/cm^3	[14]
SWCNT	tensile modulas	~1 Tpa	[1]
MWCNT	tensile modulas	~1.8 Tpa	[1,14]
MWCNT	heat conductivity	~1200 W/mk	[2]
as-grown SWCNT	surface area	100–200 m^2/g	[13, 14]
SWCNT	gas-adsorption capacity	5–10 Wt %	[7, 8]
CNT	bandgap	0.2–2.4 eV	[19]
SWCNT	type of semiconducting materials	as-grown SWCNT of p-type	[16]
MWCNT	long-term current carrying capacity	10^9–10^{10} A cm^{-2}	[15]
CNT random SWCNT film	threshold electrical field values for a 10 mA/cm^2 current density	1–3 V/μm	[17, 18]
MW(CN$_x$/C)NT field-effect transistor	electron mobility	$3.84×10^3$ cm^2/V·s	[20]
SWCNT	market	$200 per gram	[14]
MWCNT	Price of purified nanotubes	$200 per gram	[14]

the van der Waals type. The story of fullerenes and nanotubes belongs to the architecture of sp^2 bonded carbon. Due to a certain group of topological defects that can create unique, closed shell structures out of planar graphite sheets. When the size of the graphite crystallites becomes small the high density of dangling bond atoms can be formed. At such sizes, the structure does well energetically by closing onto itself and removing all the dangling bonds. Moreover, the structures formed correspond to linear chains, rings, and closed shells.

To form curved structures (such as fullerenes) from a planar fragment of hexagonal graphite lattice, certain topological defects have to be included in the structure. In the fullerene case that is done by creating pentagons. One can imagine that a greatly elongated fullerene can be formed with exactly 12 pentagons and thousands or millions of hexagons. This would correspond to a carbon nanotube. It is a long cylinder made of the hexagonal honeycomb lattice of carbon, bound by two pieces of fullerenes at the ends (Fig. 1). The diameter of the tube will depend on the size of the semi-fullerenes that the end is made of.

Nanotubes form in two categories. The first was discovered in 1991 by Iijima [13] while studying the surface of carbon electrodes used in an electric arc-discharge apparatus which had been used to make fullerenes. It presents the multi-walled carbon nanotubes (MWCNTs) made of a few to a few tens of concentric cylinders placed around a common central hollow, with
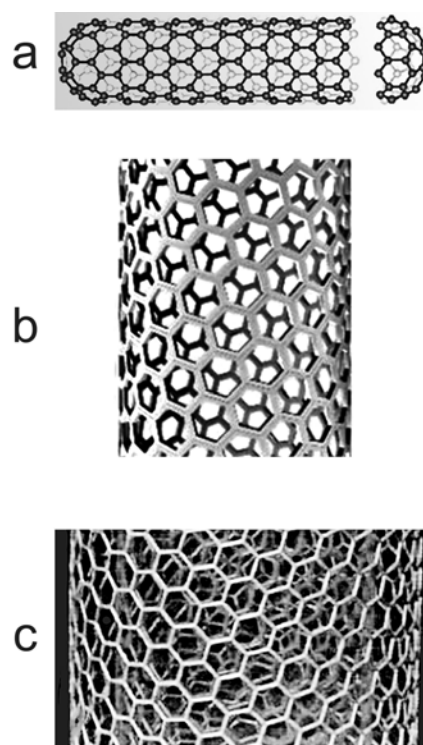
Fig. 1. Schematic of a carbon nanotube (a); single-walled CNT (b); multi-walled CNT (c).

the interlayer spacing close to that of graphite (0.34 nm) (Fig. 1c). Their inner diameter varies from 0.4 nm up to a few nm and their outer diameter ranges typically from 2 nm up to 20÷30 nm depending on the number of layers. MWCNTs usually have closed tips by insertion of pentagonal defects into the graphite network (Fig. 1a). Their axial size covers a range from 1 μm up to a few cm.

Single-wall carbon nanotubes (SWCNT), which are seamless cylinders each made of a single graphene sheet (Fig. 1b), were first reported in 1993 [5,6]. Their diameters range from 0.4 to 2-3 nm, and their length is usually of the micrometer order. SWCNTs usually come together to form bundles (ropes). In a bundle, they are hexagonally arranged to form a crystal-like structure [21].

SWCNTs can be viewed as a strip cut from an infinite graphene sheet and rolled up form a tube (Fig. 2a). The diameter and helicity of a SWCNT are uniquely characterized by the roll-up vector $\vec{C_h} = n\vec{a_1} + m\vec{a_2} \equiv (n, m)$ that connects crystallographically equivalent sites on a two-dimensional (2D) graphene sheet, where $\vec{a_1}$ and $\vec{a_2}$ are the graphene lattice vectors and n and m are integers. The limiting, achiral cases, (n, 0) zigzag, and (n, n) armchair are indicated with

dashed lines in Figure 2b. The translation vector $\vec{T}$ is along the tube axis and orthogonal to $\vec{C_h}$ and its magnitude represents the length of the unit cell of an (n,m) tube. The rolled up area swept out by $\vec{T}$ and $\vec{C_h}$ (Fig. 2b, gray) corresponds to the repeat unit of an (n, m) tube; hence, a nanotubes (n, m) symmetry determines the size of its unit cell, which can be vary greatly among tubes.

Electronic band structure calculations predict that the (n, m) indices determine whether a SWCNT will be a metal or a semiconductor [22-25]. Nanotubes made from lattice translational indices of the form (n, 0) or (n, n) will posses one plane of reflection and hence will have only two helical symmetry operations. All other sets of nanotubes will have all three equivalent helical operations. (n,0) type of nanotubes are in general called zigzag nanotubes (e.g. (8,0) nanotubes) where as the (n, n) types are called armchair nanotubes (e.g. (10,10) nanotubes) (Fig. 3). The chiral numbers m and n are definitely relating to the diameter D of SWCNTs

$$D = \sqrt{m^2 + n^2 + mn} \, \frac{\sqrt{3}d_0}{\pi}, \qquad (1)$$

where $d_0 = 0.142$ nm is the c – c bond length in the graphite plane. On the other hand, the chiral angle and chiral numbers of the SWCNT are relating each other by
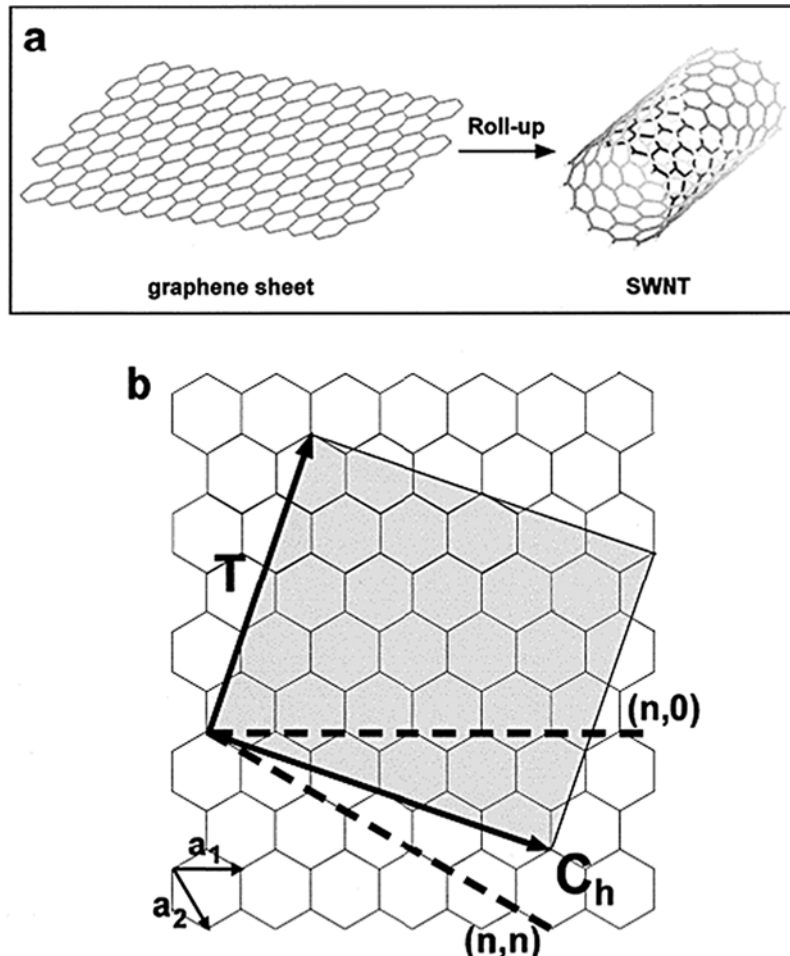
Fig. 2. (a) SWNTs can be viewed as a strip cut from an infinite graphene sheet and rolled up to form a tube. (b) Schematic of a 2D graphene sheet. The diagram is constructed for (n,m) = (4,2) [22].

means of the formula

$$\sin\alpha = \frac{3m}{2\sqrt{n^2 + m^2 + mn}},$$ (2)

or $\alpha = \tan^{-1}\left[\sqrt{3}n/(2m+n)\right]$,

α is limited to being $0 \le \alpha \le \frac{\pi}{6}$ due to the geometrical symmetry of the hexagon network and $\alpha = 0°$ for armchair nanotubes and $\alpha = 30°$ for the zigzag configuration. The nanotubes axis is aligned with two of the c – c bonds of the hexagon in the case of the (10, 10) armchair nanotube.
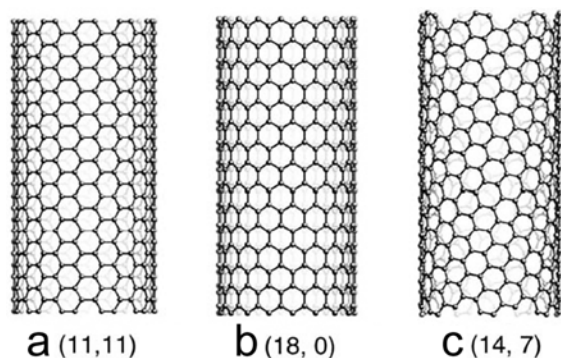
Fig. 3. Computer-generated images of single-wall carbon nanotubes [10]. Armchair type (a), zig-zag type (b), helical type (c).

Figure 4 shows a 10×10 nm² STM topography of an isolated SWCNT in three dimensions. The diameter of the nanotube can be estimated from the measured height of 0.98 ± 0.03 nm. The simultaneous atomic resolution of both the nanotube and the Si substrate suggests a very low level of contamination. The silicon dimmers and the chirality of the carbon lattice that comprises the nanotube are simultaneously resolved on this STM image.

However, as more experimental results became available, CNT was found to be not as perfect as seem.
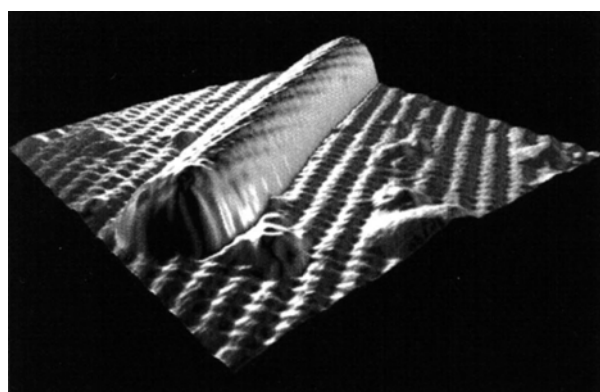
Fig. 4. Three-dimensional rendering of a 10×10 nm² STM topograph showing a single-walled carbon nanotube physisorbed onto a UHV-prepared Si(100)-2×1:H surface [25].

Defects such as the 5-7 rings, kinks, junctions, Stone-Wales defects, and impurities may be presented in as-prepared CNTs. A more interesting structural properties occurs near the ends of all tubes from the closure of the graphene cylinders by the incorporation of topological defects such as pentagons in the hexagonal carbon lattice. Complexes and structures can arise, for instance conical shaped sharp tips, due to the way pentagons are distributed near the ends for full closure. It is suggested by theory [26,29] and revealed experimentally [27] that the ends of the tubes should have different electronic structure due to the presence of topological defects. Defect induced tip electronic structure is important for several reasons. For example the field emission properties of nanotubes could be strongly influenced by the presence of localized resonant states [28]. The effect of pentagon-heptagon pair defects (widely separated defect pairs lead to surface steps) leads to the interesting possibility of changing curvature and helicity without significant bond distortions. Nanotubes with changing helicity along the axis have been reported [19].

Several out-of-plane defects can also exist in carbon nanotubes [29]. The most significant are the interfacial dislocations formed due to the helicity of individual layers and subsequent rotational disorder between the layers. Due to this, the atoms in the adjacent layers are randomized and hence the structures does not in general show three dimensional ordering that is seen in the AB stacking sequence of single-crystal graphite structures. The TEM images also manifests interfacial misfit dislocations, scrolled layers and Frank-type edge dislocations running along the axis of the tubes. The scroll formation within the tubes might explain why several adjacent cylinders in a tube could have the same helicity. Polygonized rather than perfectly cylindrical tubes have been also observed [30]. The spacing between the cylinders in each tubule also deserves mention. From the real-space analysis of images recorded from nanotubes, it is observed that a range of interlayer spacing can exist in multi-wall nanotubes (0.34-0.39 nm) [19]. In general, the spacing between cylinders increases with decreasing diameter of graphene cylinders which is due to the increasing curvature of the graphene sheets.

III. Synthesis of carbon nanotubes and purifications

The challenge now is to devise a way to mass produce SWCNTs of high purity and to control the length, diameter, and chirality. Unfortunately, it may be some time before this is realized. Arc-discharge [31] and laser vaporization [32] of carbon targets have been demonstrated as being successful for synthesis of gram quantities of nanotubes. The thermal decomposition of carbon-bearing precursors in the presence of catalysts to produce CNTs seems to be more suitable for large-scale synthesis [33-35].

Carbon nanotubes may grow under surprisingly various conditions. One distinction between the two types of nanotubes is that the MWCNTs grow with no catalysts whereas SWCNTs grow only when catalyst are present. But unlike larger catalytically grown fibers, where the fiber ends are seen decorated with catalyst particles, the ends of SWCNTs are usually closed with no trace of catalyst. During the evaporation and deposition of carbon species through the medium of arc-discharge plasma, nanotubes are formed inside rod-shaped deposits which grow at the rate of approximately 1 μm/min on the cathode surface [19,36]. The optimal experimental conditions for the growth of multi-walled nanotubes are approximately 20 V between the electrodes, a current density of 150 A/cm^2, a helium gas pressure of 500 Torr in the chamber and a constant interelectrode separation of about 1 mm. In general the anode diameter is kept, smaller than that of the cathode and both electrodes are effectively water cooled. The temperature in the interelectrode region is close to 3500ºC.

A well-advanced automated carbon-arc discharge generator with an optoelectronic control of graphite-electrode configuration and spectroscopic arrangements for plasma diagnostics is demonstrated in Ref. [37,38]. The best yield that one can obtain of carbon nanotubes and nanoparticles starting from the evaporated anode material is about 25 %.

Single-shell nanotubes were first produced by the arc discharge method through the usage of the catalyst particles along with the evaporated carbon. In this case, a hole is drilled in the center of the anode and filled in with mixtures of metal catalysts and graphite powder, the metal being 1-10% by weight. Several catalysts have been used but the best yield of nanotubes has been obtained for Ni, Co and bimetallic systems such as Ni-Y, Co-Ni, Co-Pt. The deposites contain large amounts of bundles containing 10-100 SWCNTs codeposited along with amorphous carbon and nanoparticles of the catalyst atoms. The use of a Ni-Y catalyst (in a 4 to 1 ratio) in the arc discharge has provided very high yield (>75 %) of SWCNTs [39]. Semi-continuous procedure of SWCNTs synthesis by a hydrogen arc discharge with a mixture of 2.6 at % Ni, 0.7 at % Fe, 0.7 at % Co and 0.75 at % FeS yielded more than 1.0 g of nanotubes per hour [40].

Another efficient way of producing single-walled nanotubes has also been demonstrated by using a laser evaporation technique [21,41,42]. Direct laser vaporization of transition metal-graphite (e.g. Co-Ni, 1%; Ni-Y (4.2:1, % 2:0.5,%)) composite electrode targets in helium or argon atmosphere in an oven heated to about 1200ºC (or without a furnace using a continuous-wave 250 W CO$_2$-laser operating at 10.6 μm [42] (Fig. 5)) has yielded single-walled nanotubes with a far better yield (>80 %). The amount of carbon deposited as soot is also minimized by the use of two successive laser pulses: the first to ablate the carbon-metal mixture and the second to break up the larger ablated particles and feed them into the growing nanotubes structures. Fig. 6 presents the TEM images of bundles of SWCNTs catalyzed by a Ni-
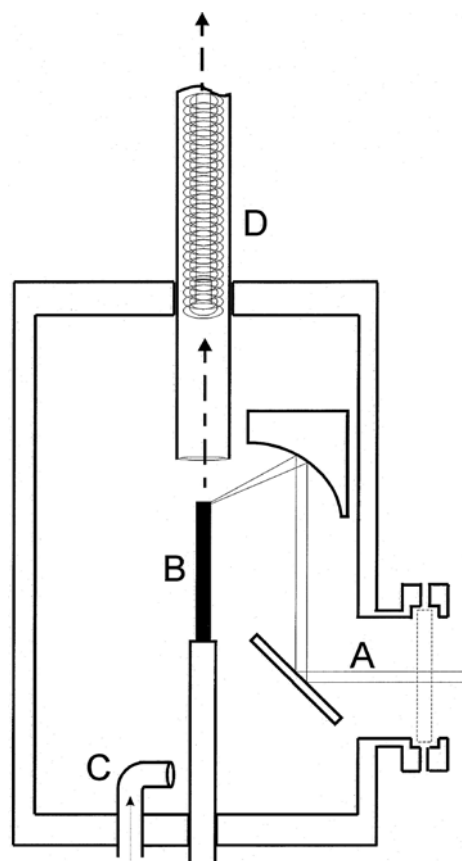
Fig. 5. The laser beam A is guided into the evaporation chamber and focused onto the graphite/metal composite target rod (B). Inert gas is introduced through a nozzle (C). Products are collected on the Cu-wire system inside the quartz tube (D) leading to the filter and pumping unit.

Y (2:0.5 at %) mixture and produced by a laser-ablation method. The arrangement of individual SWCNTs into bundles can be seen in Fig. 6 (a and b). In laser ablation and arc discharge, the yield of SWCNTs was high when NiCo catalyst was used and followed the order NiCo > Ni ~ NiFe >> Co ~ Fe > Pd ~ Pt [43]. The poor catalytic ability of Pd and Pt as graphitization catalyst caused their low catalitic activity in SWCNT formation. The high solubility of Fe in carbon leading to the low segregation temperature of Fe particles from C-Fe solution caused the low SWCNT yield when Fe was used. The instability of crystal orientation of Co on graphite is probably what hindered the steady growth of SWCNTs by the frequent changes in crystal orientation of Co when catalyzing SWCNT growth. Alternatively, it might induce fast enlargement of Co particles in a C-Co mixture at high temperatures where SWCNTs are unstable. NiCo, Ni and NiFe had high efficiencies as graphitization catalysts, low solubility in carbon and stable crystal phase and orientation on graphite. The use of a mixture of Ni and Y (4-6:1) is leading to the production a large quantity of SWCNTs by arc discharge [43].
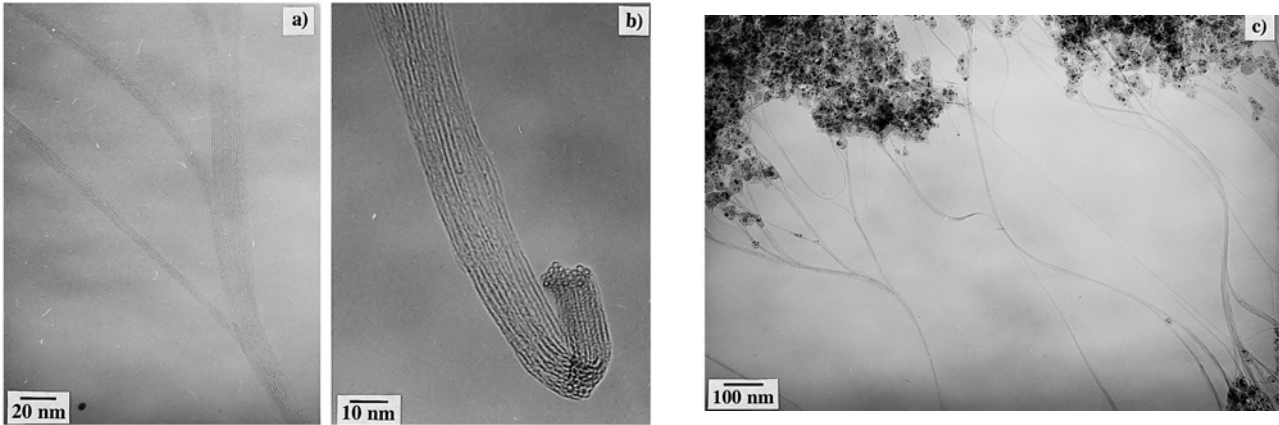
Fig. 6. TEM images of bundles of SWNTs catalyzed by a Ni/Y (2:0.5 at%) mixture. The arrangement of individual SWNTs into bundles can be seen in (a). A cross-section of such a bundle is presented in (b) while (c) shows at the merging behaviour of the bundles [42].

The production of single-walled and multi-walled CNTs over supported catalysts (Fig. 7a) or with floating catalysts (Fig. 7b) by catalytic chemical vapor decomposition (CCVD) of carbon bearing reactants have recently been reported in many papers [35,44-57]. By varying the size of the active particles on the surface of the catalyst the nanotube diameter can be tailored. This method is a widely used as a very efficient method which can be easily scaled up.

The nanotubes grow from various catalyst-impregnated substrates in the temperature range 500-1200ºC. The resulting deposits may contain a huge amount of single or multi-walled CNTs with diameters in the 1.5-20 nm range. They are usually arranged in bundles smaller than 100 nm in diameter that may be up to a few mm in length. The total number of SWCNTs in
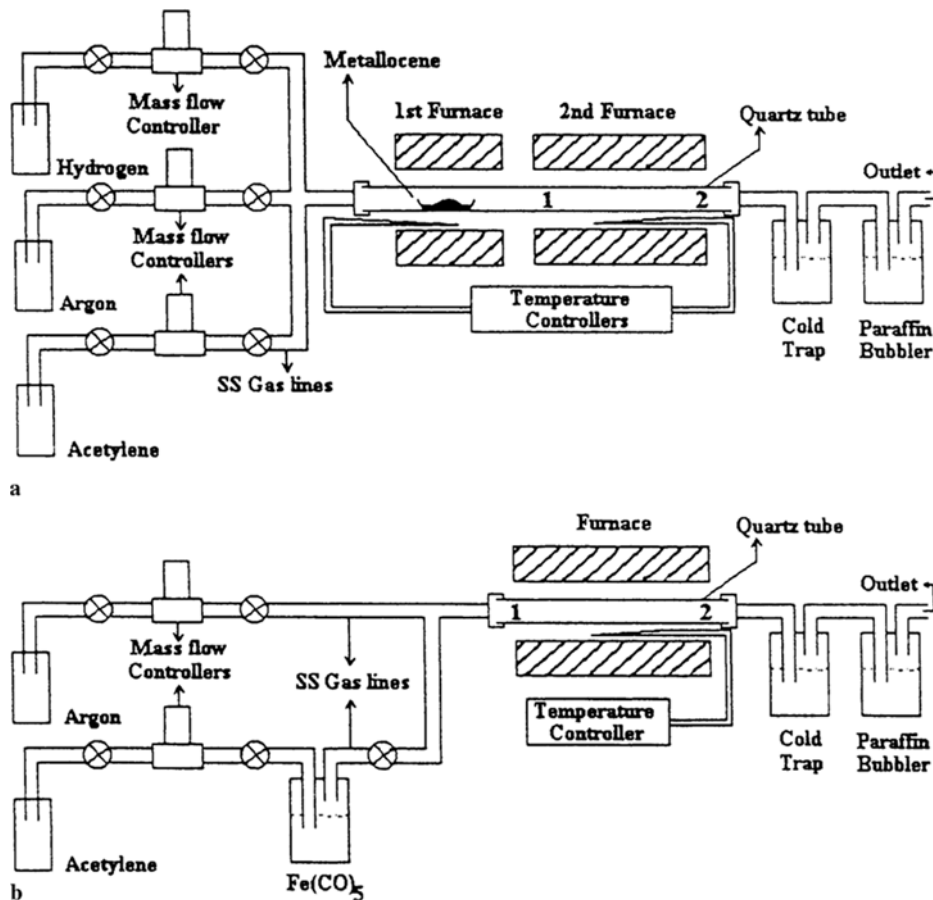
Fig. 7. Pyrolysis set-up for the synthesis of SWCNTs by CCDV of (a) metallocenes and (b) Fe(CO)$_5$ along with acetylene, [66].

such a 40 nm bundle is estimated to be 600 or more [58].

The floating catalyst method has the advantage of providing much higher yield than the seeded catalyst method because of the former continuous production [59]. The n-hexane, acetylene, high-pressure CO (HiPco), xylene are more often used as carbon containing materials. The catalyst-containing organic precursor usually ferrocene Fe(CO), is introduced in the gas phase, which also acts as an additional carbon source.

The direct synthesis of long strands (Fig. 8) of ordered SWCNTs by an optimized CCVD technique with a floating catalyst method in a vertical furnace [60,61], where n-hexane solution with a given composition of ferrocene (0.018 g ml^{-1}) and thiophene (sulfur additive 0.4 weight %) was introduced into reactor at a rate of 0.5 ml min^{-1} after heating the reactor to the pyrolysis temperature (1150ºC), with hydrogen as the carrier gas flowing at a rate of 250 ml min^{-1}.

SWCNTs yield achieves 0.5 g hour^{-1} during this continuous procedure. The formation of very long (up to 20 cm) SWCNT strands is the unique characteristic of this vertical floating process. Typically, ferrocene-assisted CVD of hydrocarbons (benzene, xylene) produces SWCNTs at T~1050 K and a mixture of single- and multi-walled nanotubes at higher temperatures (> 1300 K) [61]. The use of thiophene has been shown to increase the yield of SWCNTs. As in other procedures of SWCNTs production the strands contain impurities (~5 weight %), consisting of catalyst (Fe) particles and amorphous carbon. These strands generally have a diameter of 0.3 mm, which is larger than a human hair. The high resolution view (Fig. 8) along a single rope indicates that it consists of well-aligned bundles of SWCNTs arranged in a two-dimensional triangular lattice. The diameter of the SWCNTs varies from 1.1 to 1.7 nm.

The spectacular growth of micron-sized tree-like carbon structures produced by CVD of methane without the use of any catalysts at the temperatures of the heated graphite surface between 1100ºC and 2200ºC [89]. The deposition of carbon under extreme conditions (that is, using rapid heating and cooling cycles) can generate structures with very unusual morphologies.

All purification procedures follow certain essential steps; preliminary filtration to get rid of large graphite particles, dissolution to remove fullerenes (in organic solvents) and catalyst particles (in concentrated axids), and microfiltrations and chromatography to either size separate MWCNT and nanoparticles or SWCNT and the amorphous carbon clusters [62].

As an example, the procedures of high pressure CO SWCNTs purification [63] will be discussed shortly. Low-density raw HiPco tubes were physically compressed into a dry filter by adding SWCNTs to a filter holder while pulling a vacuum. The vacuum helps confine these lightweight samples to the filter holder. SWCNTs (typically ~ 100 mg) were placed in a ceramic boat and inserted into quartz tube furnace. A gas mixture of 20% O$_2$ in Ar (air may also be used) was passed through a water bubble and over the sample at total flow rate of 100 sccm. Nanotubes were heated at 225ºC for 18h followed by sonication for ~ 15 min or prolong stirring (overnight) in concentrated HCl solution. The tubes in the acid solution were than filtered onto a 47 mm, 1.0 µm pore size Teflon membrane and washed several times with deionized water and methanol. They were dried in a vacuum oven at 100ºC for a minimum of 2h and weighed (thermogravimetric (TGA) method). The oxidation and acid extraction cycle was repeated at 325ºC for 1.5 h and 425ºC for 1 h. After drying in the vacuum oven, the purified tubes were annealed at 800ºC in Ar to 1 h. A typical weight loss and metal concentration after each purification step is shown in Table 2. The weight loss is seen to increase dramatically from 325ºC to 425ºC step. It is found that the metal particles can be exposed with a low temperature wet Ar/O$_2$ (or wet air) oxidation step. This appears to breach the carbon shell and convert the metal particles to an oxide and/or hydroxide. The expansion (densities for Fe and Fe$_2$O$_3$ are respectively 7.86 and 5.18 g/cm^3) of the metal particle, due to the lower density of the oxide, breaks the carbon shells open and exposes the metal. This is evidenced by the ability of HCl to extract iron only after the wet Ar/O$_2$ oxidation. The exposed metal particle subsequently catalyze the oxidation of other forms of carbon and SWCNTs once the carbon shell is
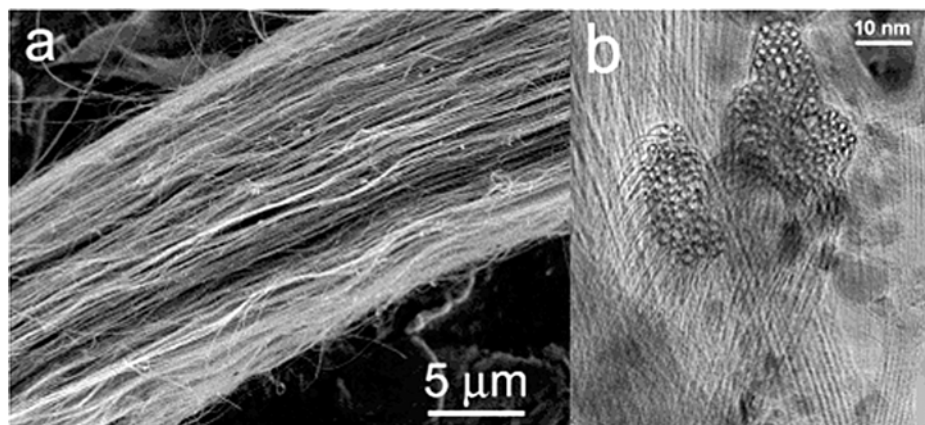
Fig. 8. Micrographs of a typical single-walled nanotube strands (a) SEM image of the strand consisting of thousands of nanotube (D = 1.1–1.2 nm) bundles; approximately 15 µm in diameter. (b) HRTEM image of a cross sectional view of single-walled nanotube bundles showing their two-dimensional triangular lattice [60].

Table 2

Weight Loss and Metal Concentration after Each Purification Step[a]

[a] Each oxidation step is followed by sonication in concentrated HCl solution for 10–15 minutes. Tubes were then filtered and dried from the acid solution in a vacuum oven at 100ºC for a minimum of 2 h.

[b] Metal % = Fe percent, which is calculated as Fe atomic percent/(C+Fe) atomic percent from the TGA data.

[c] Total weight loss = 69.1%; total weight loss excluding the 425ºC step = 46.25%

Sample	Metal %[b]	Weight loss[c]
(a) raw HiPco	5.06	
(b) raw HiPco tubes heated at 225ºC in wet Ar/O$_2$ for 18 h	0.67	33.7%
(a) heated at 325ºC in wet Ar/O$_2$ for 1.5 h	0.05	8.3%
(b) heated at 425ºC in wet Ar/O$_2$ for 1 h	0.03	22.9%
(d) annealed in Ar at 800ºC for 1 h	0.03	4.2%

removed.

IV. Building aligned carbon nanotubes and their smart architectures

Aligned nanotubes can now be produced from carbon-containing materials by various techniques including either thermal activation or plasma excitation of reactants (with or without catalysts), a nanolithographic approach and other methods. The synthesis of aligned CNTs is by far superior by comparison with laser or arc plasmas, since other undesirable carbon nanostructures are notably absent. As we have above mentioned, the chemical, physical and electronic properties of CNTs are dependent on their geometry and structure, which are determined by the preparation procedures. Recently, CNTs with different orientations and structures have been produced by adjusting the growth parameters in CVD process such as size and type of catalysts, reaction gas pressure and temperature. Tangled MWCNTs have been synthesized on SiO$_2$ supported cobalt nanoparticles [64]. Well-aligned MWCNTs have been produced on iron-embed porous silica [65], cobalt-coated silicon [66], nickel-and iron-coated glass, Al$_2$O$_3$ and Si$_3$N$_4$ [67,68] or silicon [68] by either thermal CVD [65-68] or plasma-enhanced CVD [69]. SWCNTs have been fabricated by decomposition of hydrocarbon gas such as CH$_4$ or CO over single metal catalyst such as Fe, Co, Ni [68,70-72] and alloys such as Fe-Mo [73] and Co-Mo [74].

It is found [75] that catalyst has a strong effect on the nanotube diameter, growth rate, wall thickness, morphology and microstructure. Ni yields the highest growth rate, largest diameter and thickest wall, whereas Co results in the lowest growth rate, smallest diameter and thinnest wall. The CNTs catalyzed by Ni have the best alignment and the smoothest and cleanest wall surfaces, whereas those from Co are covered with amorphous carbon and nanoparticles on the outer surface. A thinner catalyst film usually induces the formation of smaller catalyst particles and thus produces carbon nanotubes with a smaller diameter [75].

The growth and structure of CNTs are strongly affected by the temperature. The effect of temperature on growth and structure of CNTs using CVD has been investigated in the case of iron embedded silica at various temperatures from 600 to 1050ºC with gas pressure fixed at 0.6 and 760 Torr. At low gas pressure, the CNTs grown by CVD are completely hollow at low temperature and bamboo-like structure at high temperature [70]. The diameter of CNTs increases significantly with temperature. At low gas pressure the diameter gets bigger by mainly increasing the number of graphene layers of the wall of CNTs, whereas at high pressure the diameter gets bigger by increasing both the number of graphene layers of the wall and the inner diameter of the CNTs. This result indicates that the growth temperature is crucial in synthesizing CNTs with different structures.

Fig. 9 shows typical experimental system for the generation of aligned CNTs with the floating catalyst [76]. Large area of vertically aligned CNTs were synthesized on various substrates by pyrolysis of iron (II) phthalocyanine, FeC$_{32}$N$_8$H$_{16}$ (Fe Pc), under Ar/H$_2$ flow at 800-1100ºC in a dual furnace. The arrays of aligned CNTs could be generated either by patterned growth of the nanotubes on a partially masked/prepatterned surface or through a contact printing process. The micropatterned carbon nanotube growth on planar Si substrates is illustrated on Fig. 10. A patterned Fe film with a thickness of 30 nm and side lengths of 5 μm by 5 μm, 10 μm by 10 μm and 20 μm by 20 μm at a pitch distance of 15 μm, 20 μm and 30 μm, respectively has been deposited on planar Si substrates as a catalyst for CNTs growth [77]. Then micropatterned vertically aligned carbon nanotubes were grown on a planar Si surface using chemical vapor deposition. The vertical alignment of the carbon nanotubes is due to van der Waals interactions between neighboring CNTs. The tiling on Fig. 10a may be due to a reduction in van der Waals forces causing a straight alignment because of a reduction in the number of CNTs in a square pattern. The fabrication process reported here will be of great help in devolving integrated radio-frequency amplifiers or field-emission-cold-electron guns for field-emission displays.
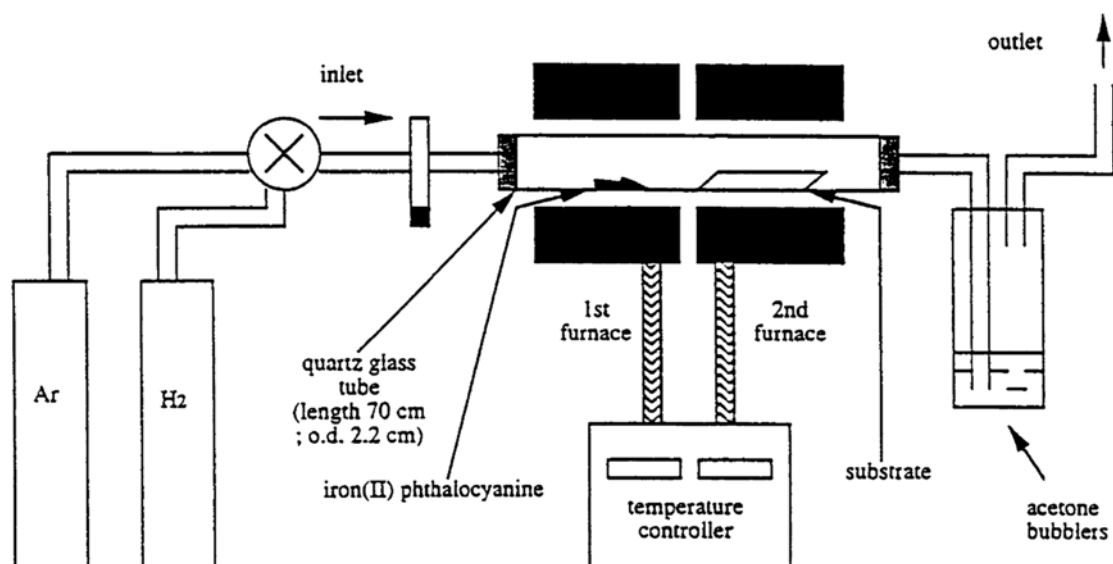
Fig. 9. The pyrolysis apparatus employed for the floating-catalyst synthesis of aligned CNTs, [76].
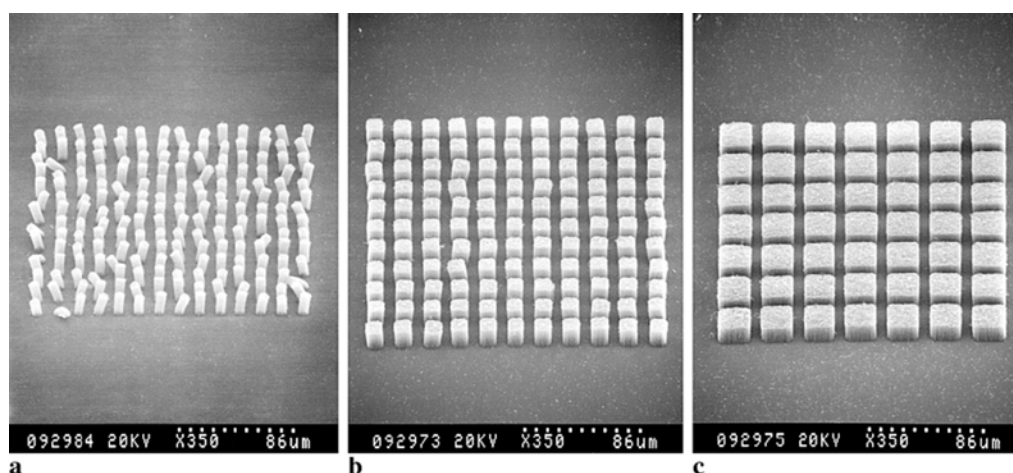
Fig. 10. Micropatterned carbon-nanotube growth on planar Si substrates [77]. (a) A pattern of 30 nm Fe film squares of side lengths of 5 μm by 5 μm at a pitch distance of 15 μm (left). (b) A pattern of squares of 10 μm by 10 μm at a pitch distance of 20 μm (center). (c) A pattern of squares of 20 μm by 20 μm at a pitch distance of 30 μm (right). CVD growth at 800°C via the pyrolysis of acetylene. The fabrication process is compatible with currently used semiconductor processing technologies.

To control over the emission current the gate electrode is used. Because of it a simple and desirable device structure is a vertical field-emission diode containing carbon nanotube field emitters in a trench (Fig. 11). The trench-fabrication process includes several layers of thin film growth, patterning and etching and the deposition of Fe catalyst on the bottom of the trench [77].

Despite the high level of control, CVD and plasma enhanced CVD (PECVD) growth typically involves processing temperatures over 500ºC, which significantly limits the choice of possible substrate materials and integration processes. For flat-panel displays and vacuum microelectronics CNTs should be deposited on glass or polymers substrates at a temperature below 300ºC. Recently it was demonstrated [78,79] low-temperature (120ºC) growth of vertically aligned CNTs arrays for field emitters onto plastic substrates ((Kapton polymide foil) and on silicon using PECVD). Field emission

measurements show a low turn-on field i.e., the field for which j is 10^{-9} A/cm^2 (3.2 V/μm) and a low threshold field i.e., the field for which j is 10^{-6} A/cm^2 (4.2 V/μm).

Another promising way to manipulate with aligned CNTs is their template synthesis [35,55,80]. When the CVD process is carried out within the pore (several nm in diameter) of a template, a carbon nanotube is formed within each pore. The template can then be dissolved leaving a free-stranding array of aligned CNTs. Polymers, metals, semiconductors and other materials have been deposited within the pores of various templates. Nearly any solid matter can in principle be synthesized within nanopores templates, provided as suitable chemical pathway can be developed. There are a few dominant methods to carry out template synthesis of nanostructures: electrochemical deposition, electroless deposition, chemical polymerization, sol-gel deposition and CVD. The template technique allows the design of a
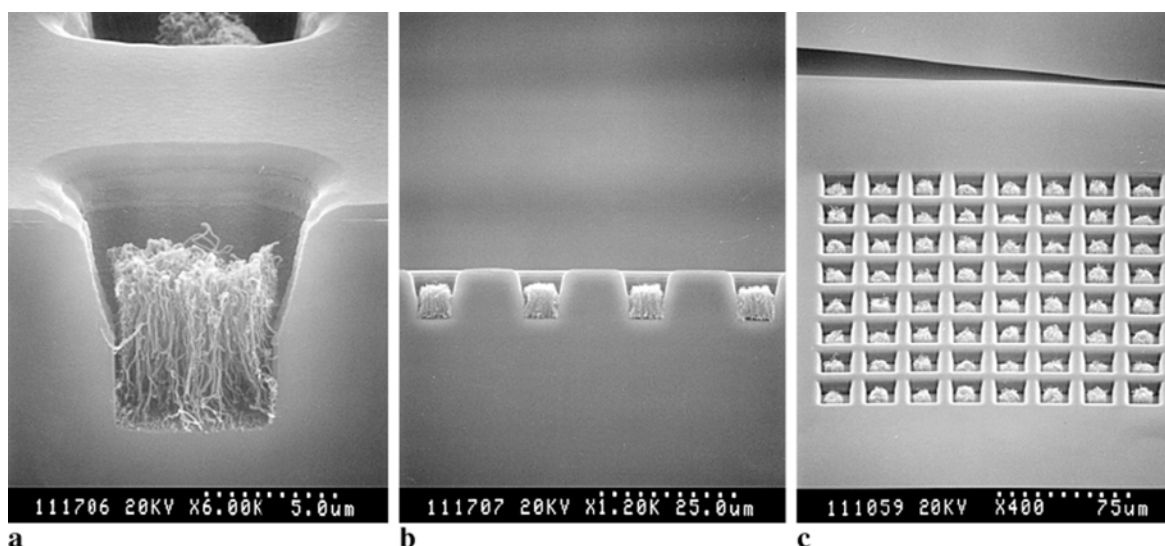
Fig. 11. SEM images of the arrays of trenches 10-μm deep with carbon nanotubes grown only on the bottom of the trenches. (a) Side view. (b) Top view. The trench fabrication process was used in order to generate a triode using CNTs and included several layers of thin film growth, patterning, etching and deposition of Fe catalysts on the bottom of the trenches [77].

wide range of novel optical and electronic devices, MEMS, biomedical chromatography, sensors, effective field emitters [80,81].

Synthetic mineral crystals, aluminophosphate AlPO$_4$-5, silica aerogels, mesopores silica and silicon, and anodic aluminum oxide (AAO) are highly porous material that have found application in CVD synthesis of aligned CNTs.

At present anode aluminum oxide (AAO) is widely used in a template-based synthesis of nanomaterials. A self-organized alumina membrane produced under certain electrochemical conditions possesses a porous structure with uniform and parallel nanopores (Fig. 12). Diameters of these pores are electrochemically tunable in the range of a few to several hundred nanometers. It is an ideal template material for creating arrays of aligned nanostructures. Pore densities as high as 10^{11} pores·cm^{-2} are obtained and typical membrane thickness can range from 10 to 150 μm. After the CVD process is accomplished, the AAO membrane can be dissolved away to axpose an ensemble of free-standing tubular nanostructures with outer diameter closely resembling the size of the pores [82,83]. Therefore, using these membranes, one can make very large panels of well-aligned CNTs that can be used as cold-cathode flat-panel displays [83,84].
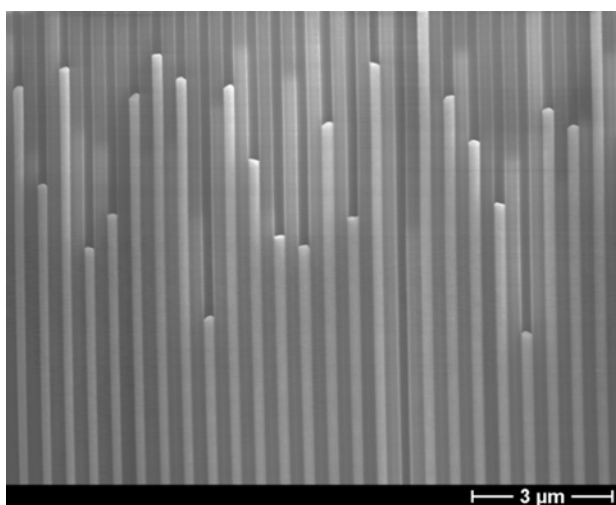
The use of soft litographic techniques for fabricating patterned and aligned arrays of CNTs open avenues for fabricating various nanodevices for a wide range of applications [85]. Growing three-dimensional architectures of carbon nanotube, which might be integrated into micoelectronic circuits, or MEMs still remains a challenge. One or two-dimensional connections and or junctions with nanotubes have fabricated by in situ growth processing and subsequent nanofabrication [86,87]. But, interconnecting nanotubes with the substrate and/or metal films is a crucial problem for realizing three-dimensional nanotube based devices up to now. As an example of successful approaches, the vertically aligned MWCNTs grow underneath the thin Ni layers, resulting in the lift of the Ni patterns from the Si substrates [88, 89]. This lift-up growth links the thin-film metal patterns and the Si substrate via nanotube assemblies, giving the possibility of creating nanotube architectures in three dimensions [90].

The Rensselayer Polytechnic Institute team [89,90] designed and built all of their nanotube structures on patterns created on silica (SiO$_2$) and silicon surfaces. Patterning of Si/SiO$_2$ was generated by standard photolithography followed by a combination of wet and/or dry etching. The patterned catalyst material was not used in this procedure. The CVD growth of CNTs of diameter 20-30 nm was stimulated by exposing the

Fig. 12. Side viewed SEM image of 500 nm-period alumina channels filled with silver.
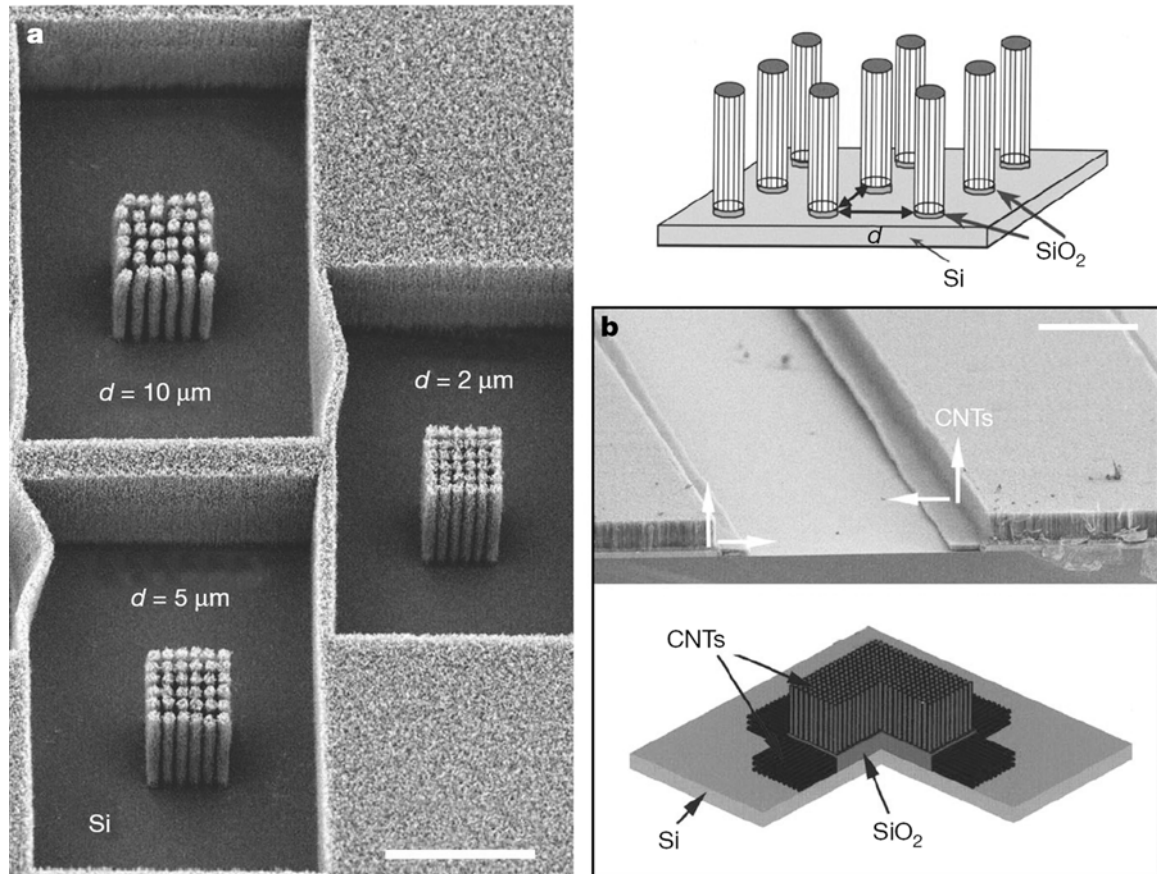
Fig. 13. (a) Image obtained by scanning electron microscopy of three blocks of cylindrical pillars (about 10 μm in diameter) of aligned carbon-nanotube arrays. Each pillar consists of several tens of nanotubes grown in vertical alignment and in a normal direction to SiO_2 patterns on the Si/SiO_2 template. No growth occurs on the Si parts of the template. The separation (*d* in diagram, top right) between pillars in the three blocks is indicated. (b) Vertical and horizontal growth of aligned nanotubes (CNTs), viewed in a cross-section of a patterned Si/SiO_2 wafer. Scale bars, 100 μm [89].

substrate to a xylene/ferrocene ($C_8H_{10}/Fe(C_5H_5)_2$) vapour mixture at around 800ºC. There is no CNTs growth on silicon, but the vertically aligned nanotubes grow perfectly on SiO_2 (Fig. 13). The simultaneous integration of ordered, geometrically varied nanotube structures in different orientations (Fig. 13) onto a single substrate could be important in the manufacture of electromechanical devices.

The fact that nanotubes grow normal to exposed SiO_2 surface suggested good possibilities of simultaneously growing arrays of CNTs that have mutually orthogonal orientation, and even arrays that are inclined at angles, using patterns of silica surfaces that are not orthogonal with the original substrate plane [90,91].

Electric fields applied nanotube growth allow the control of growth direction also [68]. The use of this effect and patterning with solid catalyst is compatible with modern semiconductor fabrication strategies and may contribute to the integration of nanotubes in complex device architectures. Recently, a controllable method (catalytic decomposition of acetylene) was developed for the synthesis of coiled nanotubes, in which aligned nanotube arrays are used as a template in order to produce asymmetric growth conditions [91,92]. These coiled nanotubes with various pitches and coil diameters show potential applications in nanoelectronics and nanomechanics.

V. CNTs characterization

After the discovery of nanotubes, initial efforts were mainly paid toward characterizing these structures. Local electron microscopy, HEED and local spectroscopy techniques have dominated the field since the spatial resolution obtained is compatible with the dimensions of nanotubes. Scanning tunneling microscopy/spectroscopy (STM/STS) has simultaneously provided atomically resolved STM topographic and current images, thereby verifying that the electronic properties of nanotubes depend on the diameter and helicity. The most conclusive evidence has been recent STM/STS studies which have shown atomically resolved lattice of nanotubes (Fig. 14) and the corresponding electronic structure of both metallic and semiconductor tubes [93-95,22,25]. Calculations [22] have predicted that all armchair tubes are metallic whereas the zigzag and helical tubes are either metallic or semiconducting. The electronic conduction process in nanotubes is unique since in the
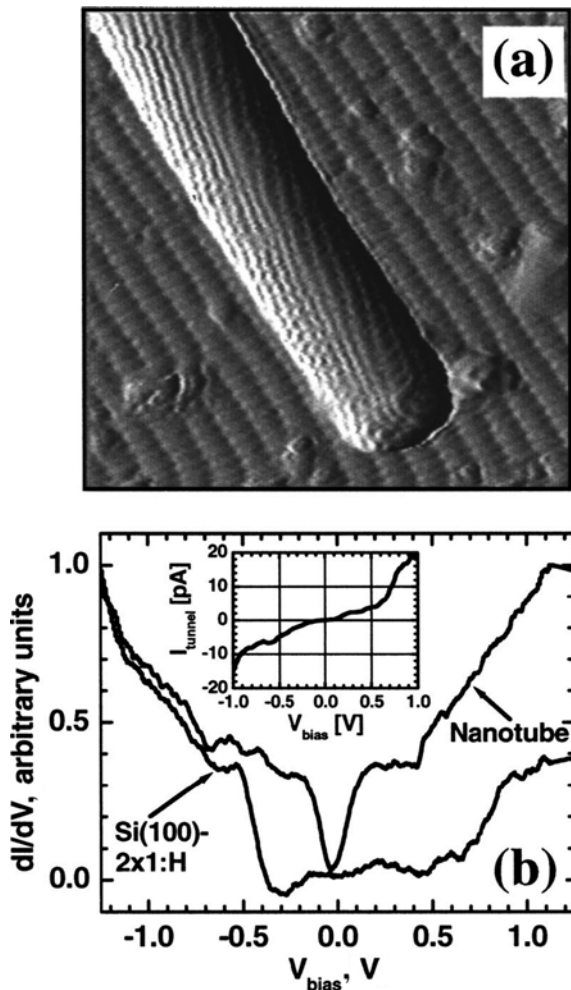
Fig. 14. (a) 10×10 nm^2 STM current image. (b) Differential conductance (dI/dV) vs sample bias (V_{bias}) for the SWNT and the substrate, respectively. The SWNT dI/dV is suppressed near the Fermi level ($\Delta V = 0.26$ V at $dI/dV = 0.3$ a.u.) Inset: Tunnel current (I_{tunnel}) vs V_{bias} for the SWNT. The curve deviates sublinearly about the Fermi level, in agreement with the small gap observed in the independently measured dI/dV characteristic [25].

radial direction the electrons are confined in the singular plane of the grapheme sheet. The conduction occurs in the armchair tubes through gapless modes as the valence and conduction bands always cross each other at the Fermi energy. In most helical tubes which contain large numbers of atoms in their unit cell, the one-dimensional band structure shows an opening of the gap at the Fermi energy, and this leads to semiconducting properties. This unique electronic behavior only occurs for small nanotubes. As the diameter of the tubes increases, the band gap (which varies inversely with the tube diameter) tends to zero. In a MWCNT, the electronic structures of the smallest inner tubes are superimposed by the outer larger planar graphene-like tubes. Experiment have indicated that the pentagonal defects present at the tips can induce metallic character by introducing sharp resonances in the local density of states near the Fermi

energy [96,97]. The field emission properties of nanotubes could be strongly influenced by the presence of localized resonant states [28]. Similar metallization of the nanotubes is also found to occur through substitutional doping of the CNTs lattice with impurities such as boron or nitrogen [98].

The experimental data on the energy gap (E_g) obtained from STM/STS measurements were presented for different chiral and zigzag tubes [22]. Significantly, these results show the expected 1/d dependence described by theoretical treatments. Moreover, these results can be used to obtain a value for the nearest neighbor overlap integral (γ_0) used in tight-binding calculations of the electronic properties by fitting to $E_g = 2\gamma_0 \, a_{c-c}/d$, where a_{c-c} is 0.142 nm. The value obtained from the one-parameter fit to the experimental results [22] is 2.5 eV. This value of γ_0 can be used in tight-binding calculations to explore self-consistently the overall electronic bend structure of SWCNTs. Analogous to E_g for, semiconducting SWCNTs, the gap between the first van Hove singularities (VHS) for metallic tubes is $E_g^m = 6\gamma_0 \, a_{c-c}/d$ [99,100], where γ_0 is the value determined from semiconducting tubes. Current vs. voltage STS measurements exhibit a linear response at $U = 0$ as expected for a metal and shows steps at larger voltages that correspond to a series of sharp peaks in the dI/dV [22,101]. These peaks correspond to the VHS resulting from the extreme points in the 1D energy bands. Therefore, these experiments provided a clear evidence of 1D band structure where peaks in density of states (Fig. 15) and van Hove singularities have been observed. Moreover, finite length nanotubes have shown a quantum confinement characteristic of particle in a box [102].

The effect of defects on transport properties in CNTs must be understood and is currently under debate. Early experiments generally assumed ballistic transport in SWCNTs. Indeed, the mean free path in individual as well in ropes of metallic SWCNTs appeared to be restricted by the contacts [103]. Later experiments, however, found evidence for defects in semiconducting NTs by using atomic force microscope tip to locally change the transport properties of the tube. Theoretical approach explained both results by stating that all defects larger than the lattice constant do not lead to backscattering within metallic tubes, whereas backscattering is present in semiconducting tubes [104]. Moreover recently, low-temperature transport measurements using individual metallic SWCNTs have been interpreted in terms of disorder-induced quantum dots [105]. According to theory, a corresponding backscattering could originate from certain arrangements of vacancies [106]. In Ref. [101] the quantized states within individual metallic SWCNTs confined by defects are registered. They appear as peaks in the dI/dV curves to close to E_F which are restricted to certain areas of the tube.

The current-carrying capacity and reliability studies of MWCNTs under high current densities up to 10^9-10^{10} A/cm^2 show no observable failure in the nanotubes structure and no measurable change in the resistance are
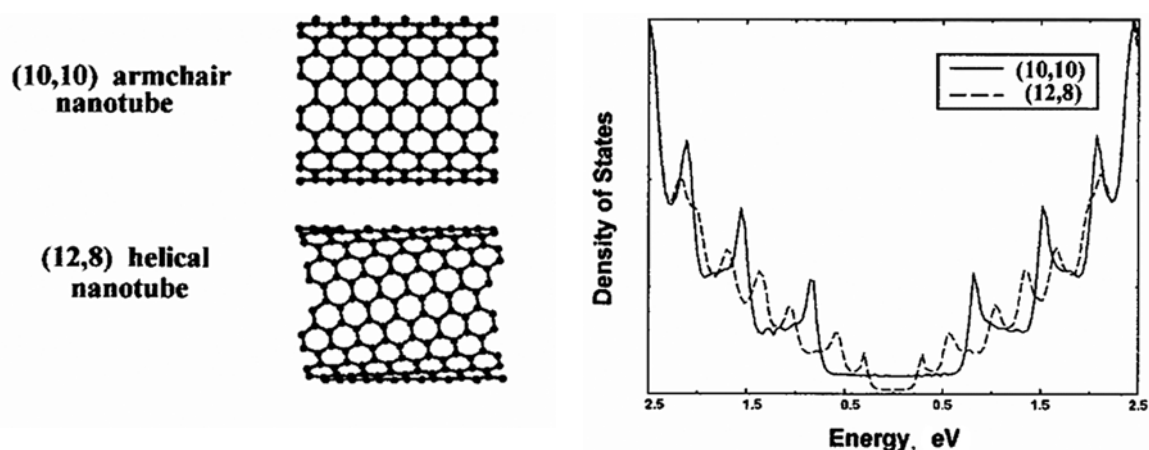
Fig. 15. Density of electronic states measured by tunneling spectroscopy over extended energy range for (10,10) armchair and (12,8) helical nanotube close to Fermi energy. A "plateu" is clearly seen for the armchair tube (metallicity) and the small gap related to the helical one [14].

registered at temperatures up to 250ºC and for time scales up to 2 weeks [15]. These results suggest that nanotubes are potential candidates as interconnects in future large-scale integrated nanoelectronic devices as they provide much higher stability against electromigration than small metallic structures. In addition experimental studies have revealed that only the outer tube in a MWCNT contributed to conductance [107].

The vibrational modes (phonons) in CNTs are extremely interesting since the spectrum varies as a function of nanotube diameter, due to changes of unit cell and the number of atoms in the unit cell with size. Some of the vibrational modes in nanotubes can be excited by Raman spectroscopy [108] (Fig. 16). The position of breathing modes in the Raman spectra (RBM) shifts with the diameter of the tubes, and this is used to determine which diameter is in resonance with the laser frequency. Such resonant Raman scattering has become a powerful tool in mapping the distribution of nanotube diameters in bulk samples [108-110]. Intertube coupling in bundles of SWCNTs causes the RBM frequency shift relative to the Raman spectra for an individual SWCNT [110]. This RBM frequency shift is influenced by the van
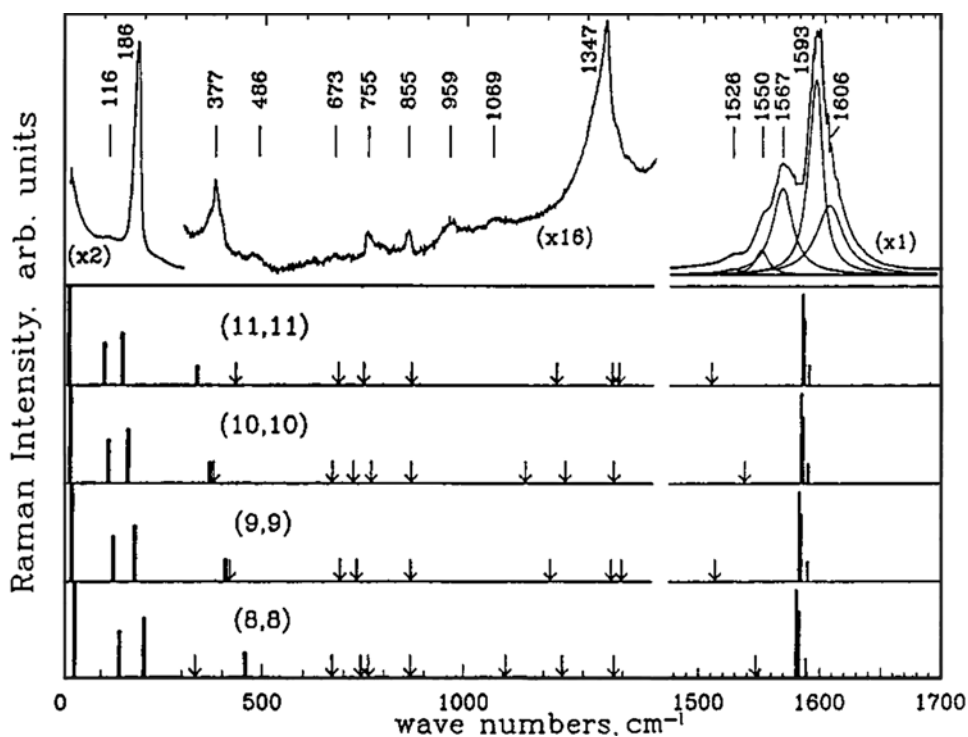
Fig. 16. Experimental Raman spectra (using 514.5 nm wavelength laser probe) from nearly pure SWNT samples showing several peaks, some of which are structure sensitive and some structure insensitive. The four bottom panels are calculations of Raman modes from nanotubes of helicity shown in brackets. Arrows show positions of weak Raman peaks [108].

der Waals interaction between the tubes. The dependence of the SWCNT diameter d and the corresponding line in the Raman spectrum ω_d is approximately described as [108] $\omega_d = 223.75 / d$.

VI. Applications

Since the discovery of the carbon nanotube by Iijima [13], research has been focused on the device-oriented applications. In particular, much success is expected from electron emission application due to the mentioned above incredible properties of CNTs such as physical strength, chemical stability, high aspect radio, and high conductivity. The creation of low-voltage field-emission display (FED) with CNT emitters is currently one of the most competitive subjects. The field emission properties of a CNT produced by different methods have been studied as from a single MWCNT [9] so from a bundle of MWCNTs [111]. Recently, Lee et al. [112] reported a 32 in panel of CNT FED with the undergate-type cathode. They used a screen-printing technique of CNT paste on a cathode to form the emitter. At this conference, Uemura et al. [113] presented a 40 in triode panel with CNT-coated cathode. Pirio et al. [114] fabricated micropatterned cathodes with CNT emitters directly formed on the bottom of the cathode holes by the PECVD at 700ºC and Y.Shiratori et al. [115,116] fabricated field emitters by the radio-frequency PECVD of vertically aligned CNTs on soda-lime glass at 400ºC.

CNT arrays on large area of AAO templates as prototype of a flat panel field emitter were deposited by CVD [83] with high emitting properties. The CNTs/AAO structures showed a low turn-on field of ~2.8 V/μm, a high maximum emitting current density of ~24 mA/cm^2, and a good emitting stability. Obraztsov et al. [117] obtained a thin-film material of oriented MWCNTs by non-catalytic CVD in a glow-discharge plasma. The excellent low-voltage electron-field emission properties of the nanotubes were observed. The emission-current density was up to 50 mA/cm^2 of the field at 5 V/μm. Compared to conventional emitters carbon nanotubes exhibit a lower threshold electric field, as illustrated in Table 3. The current densities observed from the carbon

nanotubes are significantly higher than from conventional emitters, such as nano-diamonds which tend to fail below 30 mA/cm^2 current density [17]. CNT emitters are particularly attractive for variety applications in vacuum microelectronics and for a microwave amplifier (current density of > 500 mA/cm^2).

Cathode ray lightning elements with CNT material as the field emitters have been fabricated by Ise Electronic Co. in Japan [118]. These nanotube based lighting elements have a triode-type design. Different colors are obtained by using different fluorescent materials. The luminance of the phosphor screens is two times more intense (8000 h lifetime) than that of conventional thermoionic cathode ray tube lighting elements operated under similar conditions.

Since MWCNT tips are conducting, they can be used in STM, AFM instruments as well as other scanning probe instruments, such as an electrostatic force microscope [119]. The advantage of the nanotube tip is its slenderness and the possibility to image features (such as very small, deep surface cracks), which are almost impossible to probe using the larger, blunter etched Si or metal tips. Biological molecules, such as DNA can also be imaged with high resolution using nanotube tips, compared to conventional STM tips. MWCNT and SWCNt tips were used to image biological moleculas, with resolution never achieved before [120]. It is also possible to use nanotube tips in AFM nano-lithography [18]. CNT tips look very promising in terms of wear characteristics and for improving the power efficiency in thermomechanical data storage. The demonstration of thermomechanical data storage in poly (methylmethacrylate) film using a MWCNT tip was recently presented [121]. Indentation densities of > 250 Gbits/in^2 are achieved.

Recent research has also shown that CNTs can be used as advanced chemical or biological sensors [122-123]. The electrical resistivity of SWCNTs was found to change sensitively on exposure to gaseous ambient containing molecules of NO_2, NH_3 and O_2, or to biomolecules [123]. It was seen that the response times of nanotube sensors are at least an order of magnitude faster (a few seconds for a resistance change of one order of magnitude) than those based on presently available

Table 3

Threshold electrical field values for different materials for a 10 mA/cm^2 current density (data taken from [18, 83])

Material	Threshold electrical field (V/μm)
Mo tips	50–100
Si tips	50–100
p-type semiconducting diamond	130
Amorphous diamond	20–40
Cs-coated diamond	20–30
Graphite powder (< 1 mm size)	17
Nanostructured diamond	3–5 (unstable > 30 mA/cm^2)
Carbon nanotubes	1–3 (stable at 1 A/cm^2)

metal oxide and polymer sensors. The design for CNT field-effect transistor as a chemical sensor is reported in Ref. [124].

CNTs have many potential applications as "nanopipes" for precise delivery of gases or liquids [125]. Transport rates in nanotubes are orders of magnitude faster than in the zeolites or in any microporous materials for which experimental date are available. It is a result of the inherent smoothness of the nanotubes [125].

It should be mentioned that carbon nanotubes can be effectively used as reinforcements in high strength, light weight, high performance composites (for example as spacecraft and aircraft body parts etc.) NASA has recently invested large amounts of money in developing carbon nanotube-based composites for applications such as the futuristic Mars mission [18]. There are certain advantages that have been realized in using CNTs for structural polymer (e.g., epoxy) composites. Nanotube reinforcements increase the toughness of the composites by absorbing energy during their highly flexible elastic behavior [18]. This will be especially important for nanotubes-based ceramic matrix composites. The addition of small quantities of CNTs to polymer composites is known to cause a dramatic increase in the thermal conductivity of the polymer host [125]. The thermal and electrical properties of SWCNTs-polymer composites are significantly enhanced by magnetic alignment during processing [126]. The bundling of nanotubes during the composite processing is an important factor for electrical, in particular, for thermal transport properties [126].

Since nanotubes have relatively straight and narrow channels, it was speculated from the beginning that it might be possible to fill these cavities with foreign materials to fabricate one-dimensional nanowires. Thus, nanotubes have been used as templates to create nanowires of various compositions and structures including the filling of nanotubes with metallic and ceramic materials [18]. Filled nanotubes (SiC, SiO, BN, C) can also be synthesized in situ, during the growth of nanotubes in an electric arc or by laser ablation. Decoration of nanotubes with metal particles has been achieved for different purposes [18]. Recently, an interesting application of metal-filled nanotubes, a nanothermometer based on a Ga-filled C or MgO nanotube [127-128] was realized. There are a broad range of possibilities to use the hollow space in side SWCNTs as one dimensional fields for applications in physics, electronics, chemistry and biology. Another intriguing possibility to use fulleren-incorporated nanotubes. Fulleren-incorporated nanotubes ("peapods") were recently discovered by Smith et el. in 1998 [129]. A method of producing this structure on a large scale was then developed by Bandow et al. [130]. The spin ordering inside the peapods could have a considerable impact on the development of future memory devices [10]. To our mind, such fullerene-incorporated CNTs and CNTs bundles are of great interest as a X-ray refractory

lens. The results of Kruger et al. [131] on transmission of electrons through MWCNTs showed that CNTs can be used as elements to focus electrons on the nanoscale. The electron beam was focused onto the projected center of the tube, where an amplification of the electron intensity by several times can be attained.

It was reported by Chen et al. [132] that SWCNTs-polyamide composites not only have an optical decay time of less than 1 ps, but also have a high third-order nonlinear polarizability, which make SWCNNT-polymer composite a potential material for high-quality subpicosecond all-optical switches.

Since it was experimentally shown that semiconducting carbon nanotubes can wore as field-effect transistors (EET) [133], significant progress has been made. By using thin gate dielectric films, operating voltages were reduced to around 1V [134]. It was also found that the observed p-type behavior of CNT transistors is a contact rather a bulk effect [135]. To date, a number of molecular devices have been realized with SWCNTs, including different type of FETs, room-temperature single-electron transistors [135,136], logic gate circuits [137], inverters [138-139] and electromechanical switches [140]. Very recently, the prototypes of memory devices based on SWCNT FETs were also reported [141,142]. The capability to produce n-type transistors is important technologically, as it allows the fabrication of CNT-based complementary logic devices and circuits. Experiments have shown that p- to n-type conversion of the CNT FETs can be made either by doping the surface of the tube using alkali metals, or by simply annealing the device in vacuum or in an inert gas [135].

VII. Conclusions

Carbon nanotubes have unique properties.

Unique properties lead to fabrication of different devices.

Improvements of current synthesis of carbon nanotubes needed to make available commercial products.

The totally new nanoelectronic architecture may be constructed on CNTs.

There is a little knowledge about growth mechanism, structural defects and their influence on practical properties of CNTs.

Nobel Prize laureate Prof. Smalley predicts that in the next 10 years an economical process to produce these fascinating nanostructures in ton quantities will be discovered.

There are many attractive phenomena hidden within the tiny, mysterious world that exists inside the carbon nanotube.

Fadei Komarov – Dr. Sc., Professor;
Andrej Mironov – Scientist.

[1] M.M. Treachy, T.W. Eblesen and J.M. Gibson. // *Nature,* **381**, p. 678 (1996).

[2] R.S. Ruoff, D.C. Lorents. // *Carbon,* **33**, p. 925 (1995).

[3] R. Saito, M. Fujita, G. Dresselhous and M.S. Dresselhous // *Appl. Phys. Lett,.* **60**, p. 2204 (1992).

[4] N. Hamada, S. Sawada and A. Oshiyama // *Phys. Rew. Lett.,* **68**, p. 1679 (1992).

[5] D.S. Bethunge, C.H. Klang, M.S. de Vries, G. Gorman, R. Savoy, J. Vasques and R. Beyers // *Nature,* **363**, p. 605 (1993).

[6] S. Iijima and T. Ichihashi // *Nature,* **363**, p. 603 (1993).

[7] C. Liu, Y.Y. Fan, M. Liu, H.T. Cong, H.M. Cheng, M.S. Dresselhaus // *Science,* **286**, p. 605 (1993).

[8] A.C. Dillon, K.M. Jones, T.A. Bekkedahl, C.H. Kiang, D.S. Bethune, M.J. Heben // *Nature,* **386**, p. 377 (1997).

[9] A.G. Rinzler, J.H. Hofner, P.Nikolaev, L. Lou, S.G. Kim, D. Tomanek, P. Nordlander, D.T. Colbert, R.E. Smalley // *Science,* **269**, p. 1550 (1995).

[10] S. Iijima // *Physica,* **B 323**, pp. 1-5 (2002).

[11] W.B. Choi, D.S. Chung, J.H. Kong, H.Y. Kim, Y.W. Jin, I.T. Han, Y.H. Lee, J.E. Jung, N.S. Lee, G.S. Park, J.M. Kim // *Appl. Phys. Lett.,* **75**, p. 3129 (1998).

[12] S.J. Tans, A.R.M. Verschueren, C. Dekker // *Nature,* **393**, p. 49 (1998).

[13] S. Iijima // *Nature,* **354**, p. 56 (1991).

[14] P.M. Ajayan // *Chem. Rev.,* **99**, pp. 1787-1799 (1999).

[15] R. Vajatai, B.Q. Wei, Z.J. Zhang, Y. Jung, G. Ramanath, P.M. Ajayan // *Smart. Mater. Struct.,* **11**, pp. 691-698 (2002).

[16] E.S. Snow, J.P. Novak, P.M. Campbell, D. Park // *Appl. Phys. Lett.,* **82**, pp. 2145-2147 (2003).

[17] W. Zhu, G. Kochanski, S. Jin // *Science,* **282**, p. 1471 (1998).

[18] P.M. Ajayan, O.Z. Zhou in: *Carbon Nanotubes, Topics Appl. Phys.*, Eds: M.S. Dresselhous, G. Dresselhous, Ph. Avouris, **80**, pp. 391-425 (2001).

[19] P.M. Ajayan, T.W. Ebbesen // *Rep. Prog. Phys.,* **60**, pp. 1025-1062 (1997).

[20] K. Xiao, Y. Liu, P. Hu, G. Yu, L. Fu, D. Zhu // *Appl. Phys. Lett.,* **83**, pp. 4824-4826 (2003).

[21] A. Thess, R. Lee, P. Nikolaev, H. Dai, P. Petit, J. Robert, C. Xu, Y.H. Lee, S.G. Kim, A.G. Rinzler, D.T. Colbert, G.E. Scuaeria, D. Tomanek, J.E. Fisher, R. Smalley // *Science,* **273**, pp. 483-487 (1996).

[22] T.W. Odom, J.-L. Huang, Ph. Kim, Ch. M. Lieber // *J. Phys. Chem.,* **B 104**, pp. 2794-2809 (2000).

[23] N. Hamada, S. Sawada, A. Oshiyama // *Phys. Rev. Lett.,* **68**, p. 1579 (1992).

[24] J.M. Mintmire, B.I. Dunlop, C.T. White // *Phys. Rev. Lett.,* **68**, p. 631 (1992).

[25] P.M. Albrecht, J.W. Luding // *Appl. Phys. Lett.,* **83**, pp. 5029-5031 (1992).

[26] R. Tamura, M. Tsukada // *Phys. Rev.,* **B 52**, p. 6015 (1995).

[27] D.L. Carrol, P. Redlich, P.M. Ajayan, J.C. Charlier, X. Blase, A. De Vita, R. Car // *Phys. Rev. Letters* **78**(17), pp. 2811-2814 (1997).

[28] W.A. de Heer, J.-M. Bonard, K. Fauth, A. Chatelain, L. Forro, D. Ugarte // *Adv. Mater.,* **9**, p. 87 (1997).

[29] D. Benaerts, X.B. Zhang, F. Zhang, S. Amelinickx, J. Van Landuyt, G. Van Tendeloo, V. Ivanov, J.B. Nagy // *Phil. Mag.,* **A 71**, pp. 605-630 (1995).

[30] M. Liu, J.M. Cowley // *Carbon,* **32**, pp. 393-403 (1997).

[31] T.W. Ebbesen, P.M. Ajayan // *Nature,* **358**, p. 220 (1992).

[32] J. Liu, A.G. Rinzler, H. Dai, J.H. Hafner, R.K. Bradley, P.J. Boul, A. Lu, T. Iverson, K. Shelimov, C. B. Huffman, F. Rodrigues-Macias, Y. Shon, T.R. Lee, D.T. Colbert, R.E. Smalley // *Science,* **101**, p. 1253 (1998).

[33] S. Amelinckx, X.B. Zhang, D. Bernaerts, X.F. Zhang, V. Ivanov, J.B. Nagy // *Science,* **265**, p. 635 (1994).

[34] C. Journet, P. Bernier // *Appl. Phys.*, **A 67**, p. 1 (1998).

[35] A. Huczko // *Appl. Phys.*, **A 74**, pp. 617-638 (2002).

[36] E.G. Camaly, T.W. Ebbesen // *Phys. Rev.,* **B 52**, p. 2083 (1995).

[37] H. Lange, A. Huczko, P. Byszewski // *Spectrosc. Lett.*, **29**, p. 1219 (1996).

[38] H. Lange // *Fullerene Sci. Technol.,* **5**, p. 1177 (1997).

[39] C. Journet, W.K. Maser, P. Bernier, A. Loiseau, M. Lamy de la Chapelle, S. Lefrant, P. Deniard, R. Lee, J.E. Fischer // *Nature,* **388**, pp. 756-758 (1997).

[40] C. Liu, H.T. Cong, F. Li, P.H. Tan, H.M. Cheng, K. Lu, B.L. Zhou // *Carbon,* **37**, p. 1865 (1999).

[41] T. Guo, P. Nikolaev, A. Thess, D.T. Colbert, R.E. Smalley // *Chem. Phys. Lett.,* **243**, p. 49-54 (1995).

[42] W.K. Maser, E. Munoz, A.M. Benito, M.T. Martinez, G.F. de la Fuente, Y. Maniette, E. Anglaret, J.-Z. Sauvajol // *Chem. Phys. Lett.,* **292**, p. 587-593 (1998).

[43] M. Yudasaka, Y. Kasuya, F. Kokai, K. Takanashi, M. Takisawa, S. Bandow, S. Iijima // *Appl. Phys.,* **A 74**, p. 377-385 (2002).

[44] V. Ivanov, J.B. Nagy, Ph. Lambin, A. Lucas, X.B. Zhang, X.F. Zhang, D. Bernaerts, G. Van Tendeloo, S. Amelinckx, J. Van Landuyt // *Chem. Phys. Lett.,* **223**, p. 329 (1994).

[45] K. Hernadi, P. Piedigrosso, A. Fonseca, J.B. Nagy, I. Kiricsi // *Mol. Cryst. Lig. Cryst.,* **310**, p. 179 (1998).

[46] J. Kong, A.M. Cassell, H. Dai // *Chem. Phys. Lett.,* **292**, p. 567 (1998).

[47] Z. Jia, Z. Wang, J. Ziang, B. Wei, D. Wu // *Carbon,* **37**, p. 903 (1999).

[48] E.F. Kulikowskii, L.A. Chernozatonskii, S.G. L'vov, N.N. Mel'nik // *Chem. Phys. Lett.,* **266**, p. 323 (1997).

[49] N.I. Maksimenko, O.P. Krivoruchko, A.Z. Chuvilin, L.M. Plyasova // *Carbon,* **37**, p. 1657 (1999).

[50] A.M. Benito, Y. Maniette, E. Munoz, M.T. Martinez // *Carbon,* **36**, p. 681 (1998).

[51] S. Herreyre, P. Gadelle // *Carbon,* **33**, p. 234 (1995).

[52] J. Jiao, S. Seraphin // *Chem. Phys. Lett.,* **249**, p. 92 (1996).

[53] P.E. Anderson, N.M. Rodrigues // *J. Mater. Res.*, **14**, p. 2912 (1999).

[54] L.S. Qin // J. *Mater. Sci. Lett.*, **16**, p. 457 (1997).

[55] A.V. Eletskii // *UFN (Russian),* **172**(4), pp. 401-438 (2002).

[56] P. Nikolaev, M.J. Bronikowski, R.K. Bradley, F. Rohmund, D.T. Colbert, K.A. Smith, R.E. Smalley // *Chem. Phys. Lett.,* **313**, pp. 91-97 (1999).

[57] B.C. Satishkumar, A. Govindara, R. Sen, C.N.R. Rao // *Chem. Phys. Lett.,* **293**, p. 47 (1998).

[58] A. Cao, X. Zhang, C. Xu, J. Ling, D. Wu, X. Chen, B. Wei, P.M. Ajayan // *Appl. Phys. Lett.,* **v. 79, No. 9**, pp. 1252-1254 (2001).

[59] L. Ci, B. Wei, J. Liang, C. Xu, D. Wu // *J. Mater. Sci. Lett.,* **18**, p. 797 (1999).

[60] B. Wei, R. Vajtaj, Y.Y. Choi, P.M. Ajayan // *Nano Letters,* **2**(10), pp. 1105-1107 (2002).

[61] H.W. Zhu, C.Z. Xu, D.H. Wu, B.Q. Wei, R. Vajtai, P.M. Ajayan // *Science,* **296**, pp. 884-886 (2002).

[62] P.M. Ajayan // *Chem. Rev.,* **99**, pp. 1787-1799 (1999).

[63] I.V. Chiang, B.E. Brinson, A.Y. Huang, P.A. Willis, R.H. Hauge // *J. Phys. Chem.,* **B 105**, pp. 8297-8301 (2001).

[64] V. Ivanov, A. Fonseca, J.B. Nagy, A. Lucas, P. Lambin, D. Bernaerts, X.B. Zhang // *Carbon,* **33**, p. 1727 (1995).

[65] Z.W. Pan, S.S. Xie, B.H. Chang, C.Y. Wang, L. Lu, W. Liu, W.Y. Zhou, W.Z. Li, L.X. Qian // *Nature,* **394**, p. 631 (1998).

[66] S. Fan, M.G. Chapline, N.R. Franklin, T.W. Tombler, A.M. Cassee, H. Dai // *Science,* **283**, p. 512 (1999).

[67] Y.C. Choi, Y.M. Shin, Y.H. Lee, B.S. Lee, G.S. Park, W.B. Choi, N.S. Lee, J.M. Kim // *Appl. Phys. Lett.,* **76**, p. 2367 (2000).

[68] H.B. Peng, T.G. Ristoph, G.H. Schurman, G.M. King, J. Yoon, V. Narayanamurti, J.A. Golovchenko // *Appl. Phys. Lett.,* **83**, pp. 4238-4240 (2003).

[69] C. Bower, W. Zhu, S. Jin, O. Zhou // *Appl. Phys. Lett.,* **77**, p. 830 (2000).

[70] W.Z. Li, J.G. Wen, Z.F. Ren // *Appl. Phys.*, **A 74**, pp. 397-402 (2002).

[71] J. Kong, H.T. Soh, A.M. Cassell, C.F. Quate, H. Dai // *Nature,* **395**, p. 878 (1998).

[72] J.F. Colomer, C. Stephan, S. Lefrant, G.V. Tendeloo, I. Willems, Z. Konya, A. Fonseca, Ch. Laurent, J.B. Nagy // *Chem. Phys. Lett.,* **317**, p. 83 (2000).

[73] M. Su, B. Zheng, J. Liu // *Chem. Phys. Lett.,* **322**, p. 321 (2000).

[74] B. Kitiyanan, W.E. Alvarez, J.H. Harwell, D.E. Resasco // *Chem. Phys. Lett.,* **317**, p. 497 (2000).

[75] Z.P. Huang, D.Z. Wang, J.G. Wen, M. Sennett, H. Gibson, Z.F. Ren // *Appl. Phys.,* **A 74**, pp. 387-391 (2002).

[76] S. Huang, L. Dai, A.W.H. Mau // *J. Phys. Chem.,* **B 103**, p. 4223 (1999).

[77] J.I. Sohn, S. Lee // *Appl. Phys.,* **A 74**, pp. 287-290 (2002).

[78] S. Hofmann, C. Ducati, B. Kleinsorge, J. Robertson // *Appl. Phys. Lett.,* **83**, pp. 4661-4663 (2003).

[79] S. Hofmann, C. Ducati, J. Robertson, B. Kleinsorge // *Appl. Phys. Lett.,* **83**, pp. 135-137 (2003).

[80] A. Huczko // *Appl. Phys.,* **A 70**, p. 365 (2000).

[81] L.M. Lynkov, N.I. Mukhurov. *Microstructures based on the anodic aluminium oxide technology.* Minsk, Bestprint, 216 pp. (2001).

[82] D. Routkevitchi, J. Chan, J.M. Xu, M. Moskovits // *Proc. Electrochem. Soc.,* **97**, p. 35 (1997).

[83] M. Gao, Ch. Mu, F. Wang, D. Xu, K. Wu, Y. Xie, Sh. Liu, E. Wang, J. Xu, D. Yu // *J. Appl. Phys.,* **93**, pp. 5602-5605 (2003).

[84] F. Schlottig, M. Textor, U. Deorgi, G. Roewer // *J. Mater. Sci. Lett.,* **18**, p. 599 (1999).

[85] K.H. Choi, J.P. Bourgoin, S. Auvray, D. Esteve, G.S. Duesbeg, S. Roth, M. Burghard // *Surf. Sci.,* **462**, p. 195 (2000).

[86] N.R. Franklin, H. Dai // *Adv. Mater.,* **12**, p. 890 (2000).

[87] Y.Y. Wei, G. Eres // *Appl. Phys. Lett.,* **76**, p. 3759 (2000).

[88] B. Wei, Z.J. Zhang, G. Ramanath, P.M. Ajayan // *Appl. Phys. Lett.,* **77**, pp. 2985-2987 (2000).

[89] B.Q. Wei, R. Vajtai, Y. Jung, J. Wand, R. Zhang, G. Ramanath, P.M. Ajayan // *Nature,* **416**, pp. 495-496 (2002).

[90] R. Vajtai, B.Q. Wei, Z.J. Zhang, G. Ramanath, P.M. Ajayan // *Smart. Mater. Struct.,* **11**, pp. 691-698 (2002).

[91] D.Y. Zhong, S. Liu, E.G. Wang // *Appl. Phys. Lett.,* **83**, pp. 4423-4425 (2003).

[92] K. Hernadi, L. Then-Nga, L. Forro // *J. Phys. Chem.,* **B 105**, p. 12464 (2001).

[93] J.W.G. Wildoer, L.C. Venema, A.G. Rinzler, R.E. Smalley, C. Dekker // *Nature,* **391**, p. 59 (1998).

[94] T. Odom, J. Huang, P. Kim, C. Lieber // *Nature,* **391**, p. 62 (1998).

[95]   P.M. Albrecht, J.W. Luding // *Appl. Phys. Lett.,* **83**, pp. 5029-5031 (2003).

[96]   D.L. Carroll, P. Readlich, P.M. Ajayan, J.C. Charlier, X. Blase, A. De Vita, R. Car // *Phys. Rev. Lett.,* **78**, pp. 2811-2814 (1997).

[97]   A. Hassanien, M. Tokumoto, P. Umek, D. Mihailovic, A. Mrzel // *Appl. Phys. Lett.,* **78**, pp. 808-810 (2001).

[98]   D.L. Carroll, X. Blase, J.-C. Charlier, S. Curran, Ph. Redlich, P.M. Ajayan, S. Roth, M. Ruhle // *Phys. Rev. Lett.,* **81**, p. 2332 (1998).

[99]   A. Rubio // *Appl. Phys.,* **A 68**, p. 275 (1999).

[100]   A. Rubio, D. Sanches-Porat, E. Artacho, P. Ordejon, J.M. Soler // *Phys. Rev. Lett.,* **82**, p. 3520 (1999).

[101]   Th. Maltezopoulos, A. Kubetzka, M. Morgenstern, R. Wiesendanger, S.G. Lemay, C. Dekker // *Appl. Phys. Lett.,* **83**, pp. 1011-1013 (2003).

[102]   L.C. Venema, J.W.G. Wildoer, S.J. Tans, J. W. Janssen, L.J. Hinne, T. Tuinstra, L. Kouwenhoven, C. Dekker // *Science,* **283**, p. 52 (1999).

[103]   M. Bockrath, D.H. Cobden, J. Lu, A.G. Rinzler, R.E. Smaley, L. Balents, P.L. Mc.Euen // *Nature,* **397**, p. 598 (1999).

[104]   T. Ando, T. Nakanishi, R. Saito // *J. Phys. Soc. Jpn.,* **67**, p. 2857 (1998).

[105]   M.T. Woodside, P.L. McEuen // *Science,* **296**, p. 1098 (2002).

[106]   T. Ando // *Semicond. Sci. Technol.,* **15**, R13 (2000).

[107]   A. Bachtold, C. Struuk, J.-P. Salvetat, L. Forro, T. Nussbaumer, S. Schonenberger // *Nature,* **397**, p. 673 (1999).

[108]   A.M. Rao // *Science,* **275**, p. 187 (1997).

[109]   S. Bandow, S. Asaka, Y. Saito, A.M. Rao, L. Grigorian, E. Richter, P.C. Eklund // *Phys. Rev. Lett.,* **80**, p. 3779 (1998).

[110]   L. Alvarez, A. Righi, S. Rols, E. Anglaret, J.-L. Sauvajol // *Chem. Phys. Let.,* **320**, pp. 441-447 (2000).

[111]   W.A. de Heer, A. Chatelain, D. Ugarte // *Science,* **270**, p. 1179 (1995).

[112]   C.G. Lee, J. Lee, S.Y. Wang *et al.* // *Proc. of the Ninth Int. Display Workshop*, pp. 1021-1024 (2002).

[113]   S. Uemura, J. Yotani, T. Nagasako *et al.* // *Proc. of the Ninth Int. Display Workshop*, pp. 1025-1028 (2002).

[114]   G. Pirio, P. Legagneux, D. Pribat, K.B.K. Teo, M. Chhowalla, A.J. Amaratunga, W.I. Milne // *Nanotechnology,* **13**, p. 1 (2002).

[115]   Y. Shiratori, H. Hiraoka, Y. Takeuchi, S. Itoh, M. Yamamoto // *Appl. Phys. Lett.,* **82**, pp. 2485-2487 (2003).

[116]   Q.H. Wang, A.A. Setlur, J.M. Lauerhaas, J.Y. Dai, E.W. Seelig, R.H. Chang // *Appl. Phys. Lett.,* **72**, p. 2912 (1998).

[117]   N. Obraztsov, I. Pavlovsky, A.P. Volkov, E.D. Obraztsova, A.L. Chuvilin, V.L. Kuznetsov // *J. Vac. Sci. Technol.,* **B 18**, p. 1059 (2000).

[118]   Y. Saito, S. Uemura, K. Hamaguchi // *Jpn. J. Appl. Phys.,* **37**, Z346 (1998).

[119]   H.J. Dai, J.H. Hafner, A.G. Rinzler, D.T. Colbert, R.E. Smalley // *Nature,* **384**, p. 147 (1996).

[120]   S.S. Wang, J.D. Harper, P.T. Lansbury, C.M. Lieber // *J. Am. Chem. Soc.,* **120**, p. 603 (1998).

[121]   M.A. Lantz, B. Gotsmann, U.T. Durig, P. Vettiger, Y. Nakayama, T. Shimizu, H. Tokumoto // *Appl. Phys. Lett.,* **83**, pp. 1266-1268 (2003).

[122]   J. Kong, N.R. Franklin, C. Zhou, M.C. Chapline, S. Peng, K. Cho, H. Dai // *Science,* **287**, p. 622 (2000).

[123]   A.Star, J.-C. Gabriel, K. Bradley, G. Gruner // *Nano Lett.,* **3**, p. 459 (2003).

[124]   K. Bradley, J.-Ch. P. Gabriel, A. Star, G. Gruner // *Appl. Phys. Lett.,* **83**, pp. 3821-3823 (2003).

[125]   M.J. Biercuk, M.C. Llaguno, M. Radosavljevic, J.K. Hyun, T. Jonson, J.E. Ficher // *Appl. Phys. Lett.,* **80**, p. 2767 (2002).

[126]   E.S. Choi, J.S. Brooks, D.L. Eaton, M.S. Al-Haik, M.Y. Hussaini, H. Gamestani, D. Li, K. Dahmen // *J. Appl. Phys.,* **94**, pp. 6034-6039 (2003).

[127]   Y. Guo, Y. Bando, Z. Liu, D. Golberg, H. Nakanishi // *Appl. Phys. Lett.,* **83**, pp. 2913-2915 (2003).

[128]   Y.B. Li, Y. Bando, D. Golberg, Z.W. Liu // *Appl. Phys. Lett.,* **83**, pp. 999-1001 (2003).

[129]   B.W. Smith, M. Monthioux, D.E. Luzzi // *Nature,* **396**, pp. 323-324 (1998).

[130]   K. Hirahara, K. Suenaga, S. Bandow, H. Kato, T. Okazaki, H. Shinohara, S. Iijima // *Phys. Rev. Lett.,* **85**, p. 5384 (2000).

[131]   A. Kruger, M. Ozawa, F. Banhari // *Appl. Phys. Lett.,* **83**, pp. 5056-5058 (2003).

[132]   [132].   Y.-C. Chen, N.R. Raravikar, L.S. Schadler, P.M. Ajayan, Y.-P. Zhao, T.-M. Lu, G.-C. Wang, X.-C. Zhang // *Appl. Phys. Lett.,* **81**, pp. 975-977 (2002).

[133]   S.J. Tans, A. Verschueren, C. Dekker // *Nature,* **393**, p.49 (1998).

[134]   S. Wind, J. Appenzeller, R. Martel, V. Derycke, Ph. Avouris // *Appl. Phys. Lett.,* **80**, p. 3817 (2002).

[135]   V. Derycke, R. Martel, J. Appenzeller, Ph. Avouris // *Appl. Phys. Lett.,* **80**, p. 2773 (2002).

[136]   J.B. Cui, M. Burhard, K. Kern // *Nano Lett.,* **2**, p. 117 (2002).

[137]   V. Derycke, R. Martel, J. Appenzeller, P. Auouris // *Nano Lett.,* **1**, p. 453 (2001).

[138]   X.L. Ziu, C. Lee, C.W. Zhou, J. Han // *Appl. Phys. Lett.,* **79**, p. 3329 (2001).
[139]   K. Ishibashi, D. Tsuya, M. Suzuki, Y. Aoyagi // *Appl. Phys. Lett.,* **82**, pp. 3307-3309 (2003).
[140]   [T. Rueckes, K. Kim, E. Joselevich, G.Y. Tseng, C.Z. Cheung, C.M. Lieber // *Science*, **289**, p. 94 (2000).
[141]   M.S. Fuhrer, B.M. Kim, T. Durkop, T. Brintlinger // *Nano Lett.,* **2**, p. 755 (2002).
[142]   J.B. Cui, R. Sordan, M. Burhard, K. Kern // *Appl. Phys. Lett.,* **81**, pp. 3260-3262 (2002).

Ф.Ф. Комаров, А.М. Миронов

Вуглецеві нанотрубки: сучасне і майбутнє

Інститут фізики прикладних проблем,
Білоруський державний університет, 220064,вул. Курчатова, 7, Мінськ, Білорусь,
E-mail: KomarovF@bsu.by

Розглянуто існуючі методи синтезу та вивчення вуглецевих нанотрубок. Обговорюються співвідношення між структурними властивостями та електронними, електричними, хімічними і механічними характеристиками вуглецевих нанотрубок. Вказано недавно розроблені методи вирощування загальновідомих нанотрубок із визначаними специфічними властивостями, які перспективні для масового виробництва та всесвітньо відомого використання нанотрубкових приладів. Розглядується сучасне використання нанотрубок і їх перспективи.